Cryo-electron microscopy reveals human low density lipoprotein substructure

Rik Van Antwerpen[1,*] **and John C. Gilkey**[†]

Department of Biochemistry* and Arizona Research Laboratories,† University of Arizona, Tucson, AZ 85721

Abstract In the present study, we have examined the structure of human low density lipoprotein (LDL) using cryo-electron microscopy. Human LDL particles were analyzed in a vitrified frozen-hydrated condition, without chemical fixation or any form of staining. Hence, the lipoproteins were visualized close to their native state. Contrary to current spherical models, the overall shape of human LDL is indicated to be discoidal. The observed LDL disks have a diameter of 21.4±1.3 nm and a height of 12.1±1.1 nm (mean ± standard deviation). The average volume of LDL particles in cryo-electron microscopic preparations is estimated to be 4352 nm³. This value corresponds well with the LDL volume that has been determined by sedimentation equilibrium studies [4130–4803 nm³; Kahlon et al., 1982. *Lipids.* **17:** 323–330]. Details of LDL ultrastructure, visible as a result of local differences in mass density, are indicated to reflect the distribution of protein within the lipoprotein particle. Thus, apolipoprotein B-100 (apoB) appears to form two ring-shaped structures that are organized around the perimeter of the LDL disk.—**Van Antwerpen, R., and J. C. Gilkey.** Cryo-electron microscopy reveals human low density lipoprotein substructure. *J. Lipid Res.* 1994. **35:** 2223–2231.

Supplementary key words transmission electron microscopy • cold stage • LDL • apolipoprotein B-100

Currently, the standard technique to visualize serum lipoproteins in the electron microscope is the negative staining technique (1, 2). Many studies have illustrated the value of this technique in lipoprotein research. For example, negative staining has been used to characterize lipoprotein subclasses (3–6), to verify the integrity of reconstituted lipoprotein particles (7, 8), to compare recombinant lipoprotein particles with their native counterparts (9, 10), to demonstrate the conjugation of lipoproteins with colloidal gold (11, 12), and to map the binding of specific antibodies on the lipoprotein surface (13).

The simplicity and speed of the negative staining technique have made it a popular method that has firmly established its place in lipoprotein research. Unfortunately, however, the technique is limited by the fact that it will only visualize the outlines of lipoprotein particles, leaving internal structures concealed. An additional disadvantage is that negative staining can only be used to visualize lipoprotein particles in a completely dehydrated state. Considering the plasticity of serum lipoproteins, it is conceivable that complete dehydration changes the native shape of the particles (1, 2, 14–16).

A second electron microscopic technique that has been used in the analysis of lipoprotein particles is the freeze-fracture/freeze-etch technique (1, 17–21). The major advantage of this technique is that it can be used to examine the lipoproteins in solution. However, interpretation of the freeze-etch images of lipoprotein particles has proven to be complicated (21). In addition, the freeze-fracture/freeze-etch technique can only visualize the surface of those lipoprotein parts that are exposed during the fracturing and etching process.

Cryo-electron microscopy (22) may have significant advantages over conventional electron microscopic techniques in the analysis of serum lipoproteins. Most importantly, the technique permits the direct analysis of particles in a vitrified frozen-hydrated state, without chemical fixation or any form of staining. Thus, biological samples can be analyzed very close to their native state (22, 23). Furthermore, application of the technique may provide information about the internal structure of a supra-molecular complex. To date, cryo-electron microscopy has been used in the analysis of many structures including viruses (23), actin filaments (24), microtubules (25), ribosomes (26, 27) and multi-subunit enzyme complexes (28, 29). However, the use of this technique in lipoprotein research has been limited (30, 31).

In the present study, we have used cryo-electron microscopy to analyze the ultrastructural properties of human LDL. Contrary to current spherical models, our results suggest that the overall shape of the particle is discoidal. In addition, the observed distribution of mass densities within the LDL particle suggests that apoB forms two ring-shaped structures around the perimeter of the LDL disk.

Abbreviations: apoB, apolipoprotein B-100; HDL, high density lipoprotein; LDL, low density lipoprotein; PBS, phosphate-buffered saline.

[1]To whom correspondence should be addressed.

MATERIALS AND METHODS

Lipoproteins

Human plasma LDL (1.019 and 1.063 g • ml^{-1}) was isolated by sequential ultracentrifugation (32) from pooled, freshly drawn blood samples, donated by four normolipidemic adults. The isolated LDL was washed once at a density of 1.063 g • ml^{-1}, dialyzed overnight at 4°C against 0.9% NaCl, 0.01% EDTA and stored at 4°C prior to analysis. Samples were analyzed within 3 days after isolation.

Specimen preparation

LDL concentrations were estimated using a modified Lowry assay (33). Samples were diluted in phosphate-buffered saline (PBS; 0.1 M sodium phosphate, 150 mM NaCl, 0.02% NaN_3, pH 7.0) to a protein concentration of 100–500 μg/ml before use. Colloidal gold with a diameter of 10 nm, conjugated with goat-anti-rabbit antibodies and stabilized with bovine serum albumin (Amersham, Arlington Heights, IL) was included in the samples to facilitate focusing in the electron microscope (see below). The final dilution of the gold probe was 1:10, which resulted in a slightly pink coloration of the lipoprotein solution. The subsequent specimen preparation was performed essentially according to the "perforated film method" described by Adrian et al. (23). A 4-μl LDL sample was applied to a 300-mesh copper grid with a lacey substrate composed of carbon-coated Formvar (Ted Pella Inc., Redding, CA). The grid was held with forceps during application of the LDL sample. Subsequently, most of the sample was blotted off the grid through the pores of the lacey substrate. This was done by gently moving the grid horizontally across pre-moistened Whatman no. 1 filter paper (Whatman International Ltd., Maidstone, UK). (The filter paper was moistened with the buffer used to prepare the lipoprotein solution, i.e., PBS.). The blotting process was monitored under a dissection microscope until bulk fluid was no longer present on either side of the grid. A thin film of sample then spanned the holes of the lacey substrate. Immediately after formation of this film, the sample was plunge-frozen from room-temperature into liquid propane. Plunge-freezing was performed manually by holding the grid with forceps while plunging it "edge first" into a container of liquid propane; this container (3 cm in diameter by 2 cm in height) was cooled within a larger container of liquid nitrogen. Frozen samples were transferred to a separate container of liquid nitrogen and stored until use.

The preparation of a thin film of sample in the pores of the lacey substrate is intended to result in the formation of a layer of lipoprotein suspension in which no or very few particles are superimposed. As an alternative to the use of grids with a lacey substrate, 300-mesh copper grids without the lacey substrate were used [see the "bare grid method" described by Adrian et al. (23)]. These grids generally allowed for the formation of larger and thinner films of sample. However, these films broke more easily in the electron beam, and thermal movement or "drift" of the sample complicated photographic recording of the image.

Cryo-electron microscopy

Samples were analyzed using a Gatan model 626 cryo-stage (Gatan Inc., Warrendale, PA) and a Philips EM 420 electron microscope (Philips, Eindhoven, The Netherlands), equipped with a plate camera holding 36 8.3 × 10.2 cm films. The cryo-stage was pre-cooled with liquid nitrogen to −180°C before insertion of the grid in the sample holder. Analysis of the sample in the electron microscope was performed at 120 kV and at a temperature of −164°C to −166°C. To allow recording of tilt series, the lens program of the electron microscope was set for stereo mode. The quality of the vitrified sample, i.e., the absence of hexagonal and/or cubic ice crystals in the preparation, was checked by electron diffraction. Initial screening of the preparation and the selection of holes containing thin films of ice was performed at low magnification (8,200×) and at minimum intensity of the electron beam. Subsequently, the electron microscope was set at an instrumental magnification of 18,500× or 29,000×, after which the image was focused on the edge of a hole, or on colloidal gold particles away from the area of interest. At this stage, it was checked whether or not the preparation was moving or "drifting." When drifting occurred, the electron beam was deflected, after which the preparation was re-checked for drifting at regular time intervals. Final focusing was performed, at minimum intensity of the electron beam, on the colloidal gold particles that were present in the actual area of interest. We have found that this final adjustment increases the accuracy of focusing procedures. During the recording of a tilt series, the gold particles were used to repeatedly identify the precise area of interest and to re-focus after each tilting maneuver. The photographic film (Kodak electron microscope film, Estar thick base, No. 4489 [Eastman Kodak Company, Rochester, NY]) was exposed at an instrument emulsion setting for 80 kV (i.e., the film was underexposed) and was overdeveloped for 12 min at 20°C in D-19 developer (Eastman Kodak Company) to increase contrast. The total electron dose per image was estimated to be 1000 e^- • nm^{-2}.

Measurements and calculations

Magnifications of the electron microscope were calibrated using a standard grating pattern. Photographic negatives of vitrified frozen-hydrated LDL particles were printed on Polycontrast III RC F M paper (Eastman Kodak Company) at a final magnification of 96,000 ×. Measurements of lipoprotein dimensions were performed

on these prints, using a loupe-style magnifying glass containing a measuring scale with 0.1-mm divisions (Ted Pella Inc.). The dimensions of at least 50 projections were measured, after which the average of the obtained values, plus or minus the standard deviation, was calculated.

RESULTS

Unstained, vitrified frozen-hydrated samples of human LDL possess very little amplitude contrast when viewed in the electron microscope. At focus, the particles cannot be discerned on the viewing screen of the microscope at all. At more than 10 μm underfocus, phase contrast makes the particles visible to the eye, but at these settings resolution is very poor. Because it is not always easy to focus accurately on the edge of a hole in the lacey substrate, the inclusion of colloidal gold particles as an amplitude object in the samples facilitates focusing procedures (see Materials and Methods).

As LDL particles are randomly oriented in solution, many different projections of the lipoprotein can be observed in cryo-electron micrographs of vitrified frozen-hydrated LDL samples (**Fig. 1**). These projections can be classified in at least three different groups, based on their overall shape and substructural detail (**Fig. 2**). Group I is formed by circular projections that possess a ring of relatively high density around their perimeter. The average diameter of these projections is 21.3 ± 1.3 nm. Group II consists of rectangular projections (21.4 ± 1.9 nm × 12.1 ± 1.1 nm); two bands of relatively high density, separated by a more translucent space, are observed to run parallel to the long axis of this projection. Group III contains roughly circular to oval-shaped projections (22.7 ± 1.6 nm × 15.6 ± 2.2 nm) that reveal less structural detail than the projections of groups I and II. Occasionally, the various LDL projections suggest the presence of bead-like substructures (Fig. 2). As this type of substructure is only observed at relatively high underfocus settings, the significance of this observation should be interpreted with caution (22, 23). However, the high density circle of group I projections and the two high density bands of group II projections are detectable at all underfocus settings, indicating that these structures are real and not underfocus artifacts.

To determine whether the projections of groups I–III represent different LDL subclasses, or alternatively, whether the different projections are related, we recorded images of frozen-hydrated LDL particles at tilt angles varying from −45° to +45° relative to the 0° plane of the goniometer (**Fig. 3**). The images from these tilt series clearly demonstrate that the three different types of projections can be obtained from a single LDL particle. It is shown that rectangular projections of which the long axis runs parallel to the axis of tilt (Fig. 3a, numbers 1–3) are converted to circular projections when tilted 90°. In contrast, rectangular projections of which the long axis runs perpendicular to the axis of tilt (Fig. 3a, number 4) remain rectangular when tilted 90°. Circular projections (Fig. 3a, numbers 5 and 6) are converted to rectangular projections when tilted 90°. The changes in shape of the projections at different tilt angles indicate that the overall shape of the observed LDL structure is discoidal: face views of the disk generate circular projections (group I), while side views generate rectangular projections (group II). Group III projections represent orientations of the particle at intermediate tilt angles. The average volume of the discoidal structure, calculated from the average dimensions of the LDL projections and assuming that the observed structure is cylindrical, is 4352 nm^3.

In addition to revealing the overall shape of the observed LDL structure, the tilt recordings of Fig. 3 demonstrate that the ring of relatively high density in circular projections corresponds to the two longitudinal bands in the rectangular projections. Thus, both the "top" and the "bottom" of the discoidal structure appear to contain high

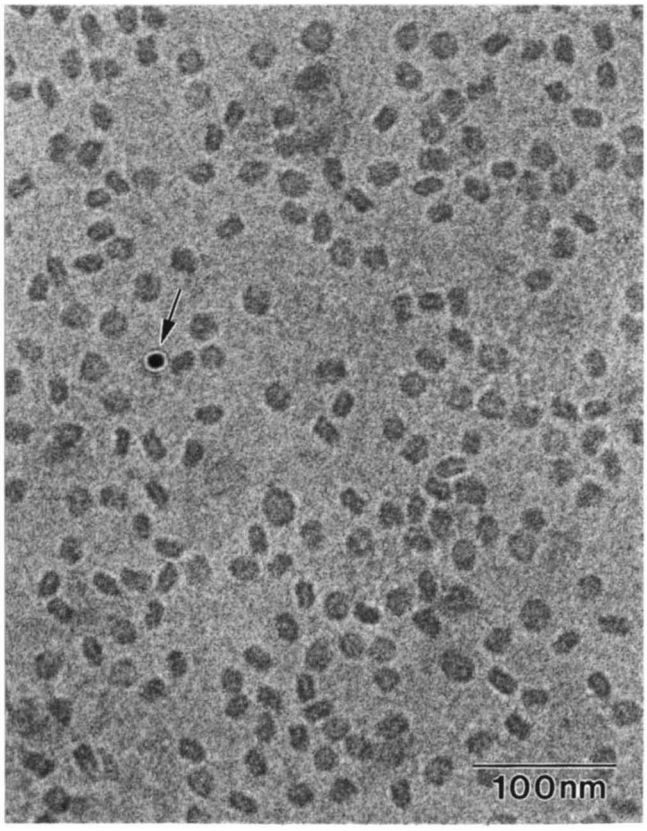

Fig. 1. Electron micrograph of vitrified frozen-hydrated human LDL. The various projections of the LDL particle can be classified in at least three groups, as shown in Fig. 2. The arrow indicates one of the colloidal gold particles (diameter ca. 10 nm) that were included in the preparation as a focusing aid. The image was recorded at an instrumental magnification of 18,500× and at 2.4 μm underfocus. Final magnification 190,000×.

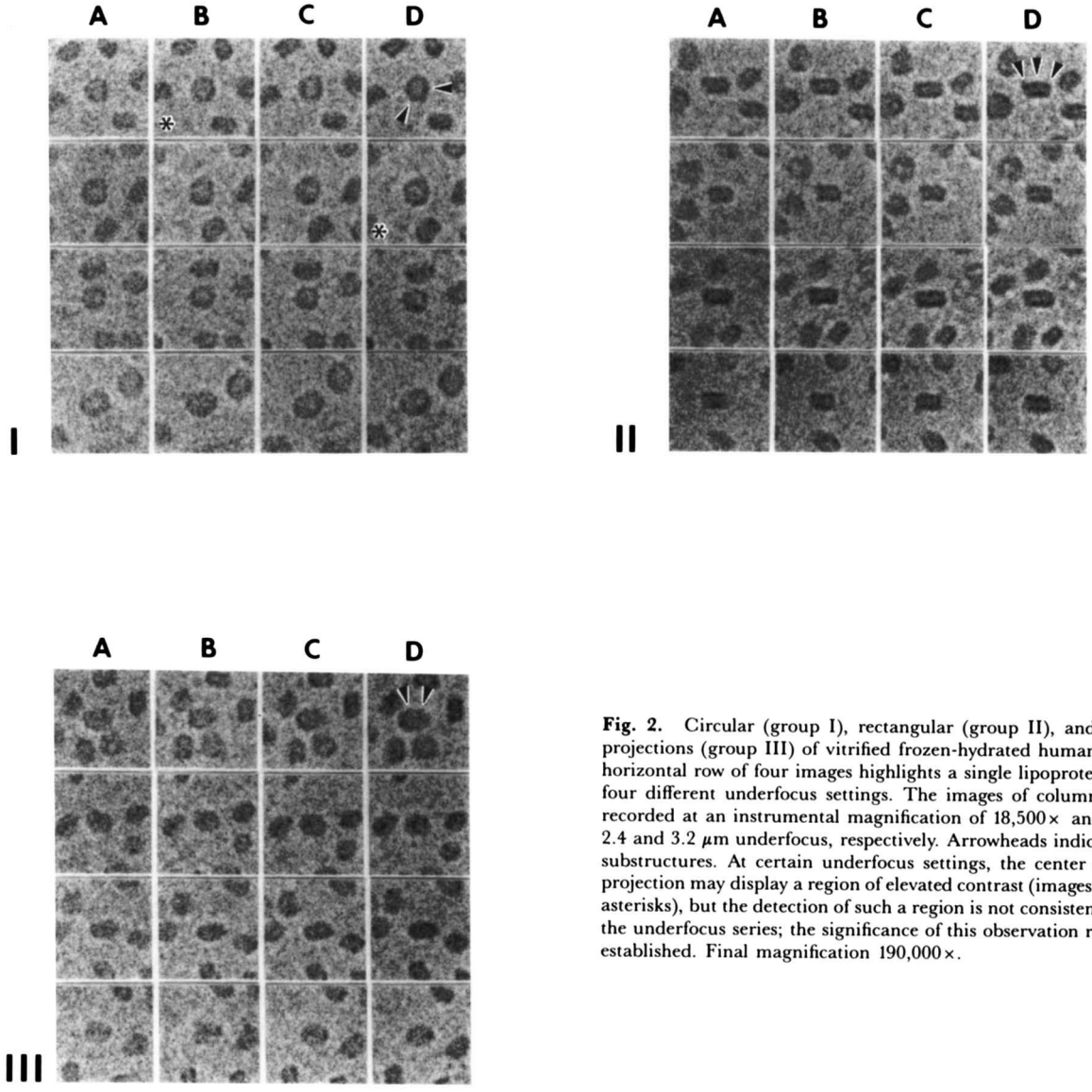

Fig. 2. Circular (group I), rectangular (group II), and oval-shaped projections (group III) of vitrified frozen-hydrated human LDL. Each horizontal row of four images highlights a single lipoprotein particle at four different underfocus settings. The images of columns A–D were recorded at an instrumental magnification of 18,500× and at 0.8, 1.6, 2.4 and 3.2 μm underfocus, respectively. Arrowheads indicate bead-like substructures. At certain underfocus settings, the center of a circular projection may display a region of elevated contrast (images marked with asterisks), but the detection of such a region is not consistent throughout the underfocus series; the significance of this observation remains to be established. Final magnification 190,000×.

density material, organized around the perimeter of the particle. In group III projections, the circular arrays of high density material are projected in such a way that less structural detail is visible.

DISCUSSION

To interpret the cryo-electron microscopic images of the present study, some fundamental aspects of image formation should be considered. Most importantly, it should be noted that the mass density of a structural element is inversely correlated with the optical density of that element in the cryo-electron micrograph (i.e., the photographic negative) (22, 23). Consequently, the contribution of different LDL components to the observed contrast can be inferred from the mass densities of these components (see **Table 1**). For example, a comparison of mass densities shows that apoB will be depicted with a lower optical density in the photographic negative than the PBS that surrounds the lipoprotein particles. Similarly, it can be deduced that domains of cholesteryl esters and triacylglycerols will be represented with a higher optical density than the background buffer, and that the contrast between domains of pure cholesterol and the background may not be detectable at all. As the different structural elements of the LDL particle are projected in the two-dimensional plane of the micrograph, domains with different mass densities may become "superimposed" during image formation, which will create an average optical density in the final micrograph. Thus, the optical density created by phospholipid molecules will depend on the orientation of

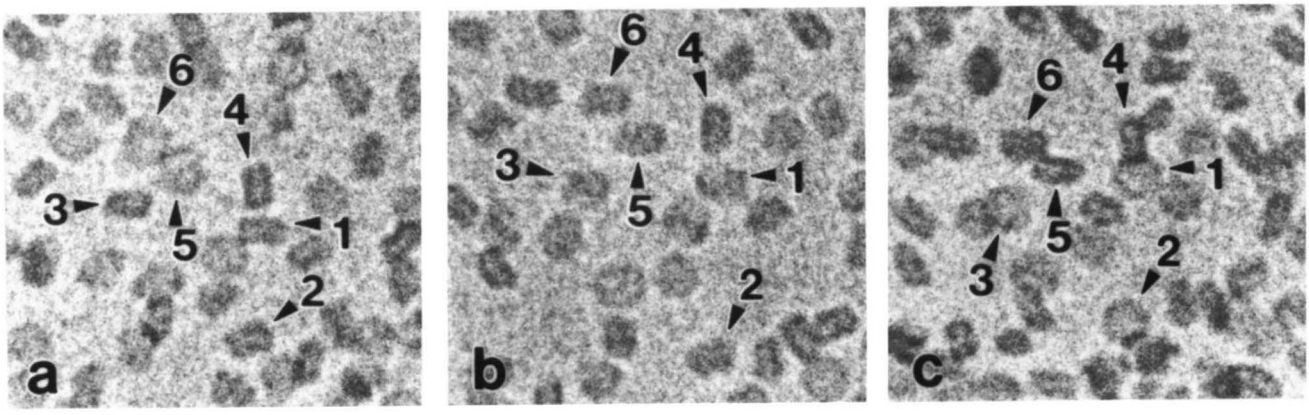

Fig. 3. Images of vitrified frozen-hydrated human LDL, recorded at goniometer tilt angles of −45° (a), 0° (b), and +45° (c). Numbered arrowheads indicate corresponding particles in each of the three views. The axis of tilt runs in a horizontal line from left to right across the figure. Note that the projected distance that a particle "moves away" from a second particle (upon tilting) will depend on the distance that separates the two particles vertically (in depth). Images were recorded at an instrumental magnification of 29,000× and at 3.2 μm underfocus. Final magnification 275,000×.

these molecules relative to the electron beam. If the beam runs perpendicular to the plane of a phospholipid monolayer, this monolayer will not be visible against a background of PBS, as the overall mass density of phospholipids is identical to the mass density of PBS. However, if the electron beam runs parallel to the plane of a phospholipid monolayer, the dense phospholipid headgroups may become visible. In conclusion, it can be stated that the observed contrast in the present images of unstained LDL is determined by *1)* the mass densities of the different LDL components, *2)* the distribution of these components in the LDL particle, *3)* the orientation of the particle relative to the electron beam, *4)* the mass density of the medium that surrounds the lipoprotein particles, and *5)* the total thickness of the preparation.

Although cryo-electron microscopy is generally thought to visualize supra-molecular structures very close to the native state (22, 23), the possible introduction of artifacts during the preparation process deserves attention. One source of artifacts may be the high surface tension forces that are present at the air–water interface on both sides of the thin film before plunge-freezing (22). These forces may orient the particles in a preferred position if the film becomes thin enough and, more importantly, they may flatten a spherical lipoprotein into a discoidal structure. The exact thickness of the ice in our preparations is unknown. However, our results at 0° tilt show that in relatively thin areas many LDL particles can be seen "edge on" (rectangular projections, group II). As tilt series demonstrate that the rectangular projections represent side views of a discoidal structure with an average diameter of 21.4 nm, it is indicated that the ice in those areas is at least 21.4 nm thick. [A typical thickness of the ice in this type of preparations is 100 nm (22).] From the optical density of the background in other areas it can be concluded that much thicker ice is also present in the sample. LDL particles in these thicker areas have the same morphology as the particles in relatively thin areas. These observations indicate that the thickness of the ice in our preparations has influenced neither the orientation nor the morphology of the particles analyzed, and exclude the possibility that surface tension forces have flattened the LDL particles.

A second type of possible artifact may be introduced by the change in temperature during ultra-rapid freezing of the lipoprotein particles. Illustrative of the possible effect of temperature on the overall structure of LDL is the phase transition of the LDL core, from a liquid state at ca. 40°C to a smectic liquid crystalline state at ca. 20°C (34–38). Thus, temperature conditions may also have an effect on the structure of the LDL particle as it is observed in our cryo-electron microscopic preparations. In the present study, LDL particles were plunge-frozen from room temperature, hence the cholesteryl ester core may

TABLE 1. Mass densities of human LDL components

Component of Human LDL	% (w/w)[a]	Mass Density[b]	Effective Mass Density[b]
		$g \cdot ml^{-1}$	
Protein	20.8	1.32[c]	0.30
Phospholipid	21.6	1.02[a]	0.00
Cholesterol	10.6	1.03[a]	0.01
Cholesteryl ester	42.4	0.96[a]	−0.06
Triglyceride	4.6	0.92[a]	−0.10

The effective mass density of each LDL component is the actual mass density of that component minus the mass density of the buffer, i.e., 1.02 $g \cdot ml^{-1}$.

[a] From Müller et al. (34).

[b] Values are mass densities at 20°C.

[c] Density of hydrated protein.

have been in a smectic liquid crystalline state before freezing (34–38). Whether the condition of the lipid core and the distribution of other lipid components within the LDL particle at room temperature are preserved during ultrarapid freezing is unknown. However, electron diffraction demonstrates that our LDL preparations are preserved in a vitrified condition, indicating that the cooling rate during plunge-freezing was around $10^{6\circ}$ C $\cdot s^{-1}$ and that fixation of structure occurred within 10^{-4} s (22, 39). Cryo-electron microscopic studies with phospholipid model membranes have demonstrated that this cooling rate is fast enough to preserve characteristic lipid phases when preparations are plunge-frozen from above phase transition temperatures (40, 41). These observations suggest that the organization of lipids in our frozen-hydrated LDL preparations is likely to be preserved close to the organization at room temperature.

The series of tilted LDL images of the present study strongly indicate that the overall shape of the observed structure is discoidal (Fig. 3). Considering the role of mass density in image formation, it seems likely that some of the lipid components of LDL are not visible in the electron micrographs. Hence, the human LDL particle could have an overall shape that differs from the observed LDL structure. However, the estimated average volume of the observed structure (4352 nm^3) is in excellent agreement with the total volume of LDL that has been determined in sedimentation equilibrium studies (i.e., 4130-4803 nm^3) (42). This indicates that all components of the LDL particle are contained within the structure that is observed in our cryo-electron micrographs. Considering the above, we conclude that human LDL may well be a discoidal particle with an average diameter of 21.4 ± 1.9 nm and an average height of 12.1 ± 1.1 nm. It should be noted that the observed LDL disk is much "thicker" than nascent high density lipoprotein (HDL) disks (4, 5): while the central part of a nascent HDL disk is basically a phospholipid bilayer, the discoidal LDL structure is thick enough to accommodate a cholesteryl ester/triacylglycerol core.

It should be noted that not all particle projections in frozen-hydrated LDL preparations show the conversion of circular to rectangular, or vice versa, upon tilting. This is not surprising, considering the fact that the particles are oriented randomly relative to the electron beam; many orientations of a discoidal particle will reveal neither a circular (group I) nor a rectangular (group II) projection at any of the three tilt angles used. In fact, many of the non-rectangular and non-circular projections resemble the "intermediate" projections that are identified as such in the tilt series. Although the observed projections, and the way these projections change shape upon tilting, strongly suggest a discoidal shape of the observed LDL structure, it cannot be excluded that some particles in the preparation possess a non-discoidal organization.

The inverse correlation between the mass density of a structure and its optical density in a cryo-electron micrograph may provide a basis for the visualization of apolipoproteins within a lipoprotein particle. In the present case of human LDL, several considerations indicate that the high density circle in group I projections and the two high density bands in group II projections correspond to apoB. *1)* As apoB has a substantially higher mass density than any of the other constituents of LDL, the protein will create the lowest optical density in photographic negatives of unstained LDL (i.e., the highest density in the final prints). *2)* The bead-like features of the high density structure may represent globular domains. This type of structural arrangement is in agreement with the suggested organization of apoB in distinct domains (13, 43, 44). *3)* There is general agreement that the core of LDL contains cholesteryl esters and triacylglycerols (34–38). This concurs with the fact that group I projections (see Fig. 2) reveal the presence of a relatively translucent LDL center. *4)* It has been shown that the buoyant density and size of nascent LDL particles depends on the length of the apoB molecule (10, 45). This is understandable if apoB defines the circumference of the LDL particle. *5)* It has recently been demonstrated that the protein moiety of LDL, after cross-linking and subsequent extraction of lipid, has a circular conformation (13, 46). This is in excellent agreement with the circular organization of high density structures in our cryo-electron micrographs.

It should be noted that phospholipid head groups may contribute to the high density structures that are observed in our cryo-electron micrographs. Specifically, if a phospholipid monolayer is present on both the top and the bottom of the discoidal structure, the head groups may contribute to the high density bands that are observed in the rectangular projections. The width of these bands, however, seems to exclude the possibility that their density is generated by phospholipid head groups only. Hence, the density distribution in rectangular (group II) projections of the LDL particle strongly suggests that apoB is associated with both the top and the bottom of the discoidal structure.

Based on the above, it is indicated that apoB forms two ring-shaped structures that are organized around the perimeter of the LDL disk: one ring associated with the top of the disk, the other ring associated with the bottom. In addition, the possible presence of globular domains within the apoB molecule is indicated. This organization of apoB would be in agreement both with the circular organization of delipidated apoB (13, 46) and with the mapping of antibody binding sites on the LDL surface (13). The mapping studies, as reported by Chatterton et al. (13), indicate that apoB wraps around the particle for at least 72% of a full turn. Based on the epitope map and on the restricted movement of epitope domains relative to each other, the authors have suggested that "apoB is prob-

ably composed of a chain of domains connected by flexible chain." Thus, it seems possible that the flexible parts of apoB connect more compact domains on either side of the LDL disk. ApoB has been demonstrated to possess distinct protease-accessible and protease-inaccessible domains (43, 44) and one of these domains has been demonstrated to contain the binding site that interacts with the LDL receptor (44). Interestingly, both the recognition of this receptor binding site by a specific monoclonal antibody as well as the receptor-lipoprotein interaction itself are abolished by a decrease in size of the human LDL particle (47). This indicates that the conformation of apoB domains changes, depending on the size of the lipoprotein particle. Using cryo-electron microscopy in future studies, it may be possible to visualize major conformational changes within apoB and to map the receptor binding site, as well as other epitopes, in situ on the apoB molecule.

The present cryo-electron microscopic images of human LDL are very different from images of LDL in negatively stained preparations (1, 2, 6, 13). The main reason for this is that the cryo-electron micrographs reveal internal structures of the LDL particle, whereas images of negatively stained LDL show only the lipoprotein's outlines. In addition to the differences in substructural detail, a discoidal shape of normal LDL particles as observed in our cryo-electron micrographs is not immediately obvious in negatively stained preparations. This may have two reasons. First, negative staining procedures require the adsorption of lipoproteins to a solid substrate; if discoidal LDL particles are adsorbed in a preferred position, i.e., lying flat on the supporting substrate, detection of a discoidal shape may not be possible. Instead, it will be tempting to conclude from the circular views of the disk that the particles are quasi-spherical. Second, negative staining procedures require complete dehydration of the lipoprotein particles in the presence of heavy metal salts. Considering the plasticity of LDL, both adsorption and complete dehydration may deform the lipoprotein particles (1, 2, 13-16). Because adsorption and dehydration are avoided in cryo-electron microscopy, the images of the present study are more likely to reflect the native state of human LDL.

While freeze-etch electron microscopy provides information about the surface features of LDL, cryo-electron microscopy visualizes both internal and surface structures. Thus, the two techniques may complement each other in giving a total picture of human LDL in a vitrified frozen-hydrated state. It seems possible that the "knobby" appearance of the LDL surface in freeze-etch preparations (18, 19, 21) corresponds with the globular domains that are observed in our cryo-electron micrographs; if these globular domains protrude from the lipoprotein's surface they may be detectable in replicas of the freeze-etched samples. However, in the present study, there are no indications of a tetrahedral organization of globular domains. Hence, our results appear to be in disagreement with the tetrahedral model of LDL structure, as described by Aggerbeck et al. (18, 19, 37).

The present study demonstrates that cryo-electron microscopy may be a valuable new technique in the analysis of serum lipoprotein structure. A major advantage of the technique is that it permits the direct visualization of lipoprotein particles close to their native state. Moreover, it is indicated that cryo-electron microscopy may visualize the distribution of apolipoproteins within a lipoprotein particle. To date, this type of structural information cannot be obtained by any other means. The present data should, therefore, stimulate comparative cryo-electron microscopic studies, the results of which may help to improve our understanding of the structural principles that govern human lipoprotein metabolism.

The authors thank Dr. Donald J. McNamara for the donation of human LDL samples and Drs. John H. Law and José Soulages for stimulating discussions. This work was supported by grants GM29238 and GM50551 of The National Institutes of Health.

Manuscript received 4 March 1994 and in revised form 30 June 1994.

REFERENCES

1. Forte, T., and A. V. Nichols. 1972. Application of electron microscopy to the study of plasma lipoprotein structure. *Adv. Lipid Res.* **10:** 1-41.
2. Forte, T. M., and R. W. Nordhausen. 1986. Electron microscopy of negatively stained lipoproteins. *Methods Enzymol.* **128:** 442-457.
3. Forte, T., R. K. R. Norum, J. A. Glomset, and A. V. Nichols. 1971. Plasma lipoproteins in familial lecithin:cholesterol acyltransferase deficiency: structure of low and high density lipoproteins as revealed by electron microscopy. *J. Clin. Invest.* **50:** 1141-1148.
4. Hamilton, R. L., M. C. Williams, C. J. Fielding, and R. J. Havel. 1976. Discoidal bilayer structure of nascent high density lipoproteins from perfused rat liver. *J. Clin. Invest.* **58:** 667-680.
5. Green, P. H. R., A. R. Tall, and R. M. Glickman. 1978. Rat intestine secretes discoid high density lipoprotein. *J. Clin. Invest.* **61:** 528-534.
6. Shen, M. M. S., R. M. Krauss, F. T. Lindgren, and T. F. Forte. 1981. Heterogeneity of serum low density lipoproteins in normal human subjects. *J. Lipid Res.* **22:** 236-244.
7. Ginsburg, G. S., M. T. Walsh, D. M. Small, and D. Atkinson. 1984. Reassembled plasma low density lipoproteins. Phospholipid-cholesterol ester-apoprotein B complexes. *J. Biol. Chem.* **259:** 6667-6673.
8. Walsh, M. T., and D. Atkinson. 1986. Reassembly of low-density lipoproteins. *Methods Enzymol.* **128:** 582-608.
9. Spring, D. J., S-M. Lee, D. L. Puppione, M. Phillips, J. Elovson, and V. N. Schumaker. 1992. Identification of a neutral lipid core in a transiently expressed and secreted lipoprotein containing an apoB-48-like apolipoprotein. *J. Lipid Res.* **33:** 233-240.

10. Spring, D. J., L. W. Chen-Liu, J. E. Chatterton, J. Elovson, and V. N. Schumaker. 1992. Lipoprotein assembly. Apolipoprotein B size determines lipoprotein core circumference. *J. Biol. Chem.* **267:** 14839–14845.
11. Handley, D. A., C. M. Arbeeny, L. D. Witte, and S. Chien. 1981. Colloidal gold-low density lipoprotein conjugates as membrane receptor probes. *Proc. Natl. Acad. Sci. USA.* **78:** 368–371.
12. Robenek, H., and N. J. Severs. 1984. Double labeling of lipoprotein receptors in fibroblast cell surface replicas. *J. Ultrastruct. Res.* **87:** 149–158.
13. Chatterton, J. E., M. L. Phillips, L. K. Curtiss, R. W. Milne, Y. L. Marcel, and V. N. Schumaker. 1991. Mapping apolipoprotein B on the low density lipoprotein surface by immunoelectron microscopy. *J. Biol. Chem.* **266:** 5955–5962.
14. Serwer, P. 1977. Flattening and shrinkage of bacteriophage T7 after preparation for electron microscopy by negative staining. *J. Ultrastruct. Res.* **58:** 235–243.
15. Frank, J. 1979. Image analysis in electron microscopy. *J. Microsc.* **117:** 25–38.
16. Frank, J., A. Verschoor, and T. Wagenknecht. 1985. Computer processing of electron microscopic images of single macromolecules. *In* New Methodologies in Studies of Protein Configuration. T. T. Wu, editor, Van Nostrand Reinhold, New York. 36–89.
17. Ohtsuki, M., C. Edelstein, M. Sogard, and A. Scanu. 1977. Electron microscopy of negatively stained and freeze-etched high density lipoprotein-3 from human serum. *Proc. Natl. Acad. Sci. USA.* **74:** 5001–5005.
18. Gulik-Krzywicki, T., M. Yates, and L. P. Aggerbeck. 1979. Structure of serum low-density lipoprotein. II. A freeze-etching electron microscopy study. *J. Mol. Biol.* **131:** 475–484.
19. Aggerbeck, L. P., M. Yates, and T. Gulik-Krzywicki. 1980. Freeze-etching electron microscopy of serum lipoproteins. *Ann. NY Acad. Sci.* **348:** 352–364.
20. Gulik, A., L. P. Aggerbeck, J. C. Dedieu, and T. Gulik-Krzywicki. 1982. Freeze-fracture electron microscopic analysis of solutions of biological molecules. *J. Microsc.* **125:** 207–213.
21. Aggerbeck, L. P., and T. Gulik-Krziwicki. 1986. Studies of lipoproteins by freeze-fracture and etching electron microscopy. *Methods Enzymol.* **128:** 547–472.
22. Dubochet, J., M. Adrian, J-J. Chang, J-C. Homo, J. Lepault, A. W. McDowall, and P. Schulz. 1987. Cryo-electron microscopy of vitrified specimens. *Q. Rev. Biophys.* **21:** 129–228.
23. Adrian, M., J. Dubochet, J. Lepault, and A. W. McDowall. 1984. Cryo-electron microscopy of viruses. *Nature.* **308:** 32–36.
24. Trinick, J., J. Cooper, J. Seymour, and E. H. Egelman. 1985. Cryo-electron microscopy and three-dimensional reconstruction of actin filaments. *J. Microsc.* **141:** 349–360.
25. Mandelkow, E-M., R. Rapp, and E. Mandelkow. 1985. Microtubule structure studied by quick freezing: cryo-electron microscopy and freeze fracture. *J. Microsc.* **141:** 361–373.
26. Wagenknecht, T., R. Grassucci, and J. Frank. 1988. Electron microscopy and computer image averaging of ice-embedded large ribosomal subunits from *Escherichia coli*. *J. Mol. Biol.* **199:** 137–147.
27. Frank, J., P. Penczek, R. Grassucci, and S. Srivastava. 1991. Three-dimensional reconstruction of the 70S *Escherichia coli* ribosome in ice: the distribution of ribosomal RNA. *J. Cell Biol.* **115:** 597–605.
28. Wagenknecht, T., R. Grassucci, and D. Schaak. 1990. Cryo-electron microscopy of frozen-hydrated α-ketoacid dehydrogenase complexes from *Escherichia coli*. *J. Biol. Chem.* **265:** 22402–22408.
29. Wagenknecht, T., R. Grassucci, G. A. Radke, and T. E. Roche. 1991. Cryo-electron microscopy of mammalian pyruvate dehydrogenase complex. *J. Biol. Chem.* **266:** 24650–24656.
30. Atkinson, D. 1988. Electron microscopy of unstained frozen hydrated low density lipoprotein (LDL). *Arteriosclerosis.* **8:** 598A.
31. Spin, J. M., and D. Atkinson. 1993. Structure of low density lipoprotein in vitreous ice. *Biophys. J.* **64:** A286.
32. Mills, G. L., P. A. Lane, and P. K. Weech. 1984. The isolation and purification of plasma lipoproteins. *In* Laboratory Techniques in Biochemistry and Molecular Biology: A Guidebook to Lipoprotein Techniques. Elsevier Science, Inc., New York. 55–73.
33. Peterson, G. L. 1983. Determination of total protein. *Methods Enzymol.* **91:** 95–119.
34. Müller, K., P. Laggner, O. Glatter, and G. Kostner. 1978. The structure of human-plasma low-density lipoprotein B. An X-ray small-angle scattering study. *Eur. J. Biochem.* **82:** 73–90.
35. Deckelbaum, R. J., G. G. Shipley, and D. M. Small. 1977. Structure and interactions of lipids in human plasma low density lipoproteins. *J. Biol. Chem.* **252:** 744–754.
36. Atkinson, D., R. J. Deckelbaum, D. M. Small, and G. G. Shipley. 1977. Structure of human plasma low density lipoproteins: molecular organization of the central core. *Proc. Natl. Acad. Sci. USA.* **74:** 1042–1046.
37. Luzatti, V., A. Tardieu, and L. P. Aggerbeck. 1979. Structure of serum low-density lipoprotein. I. A solution X-ray scattering study of a hyperlipidemic monkey low-density lipoprotein. *J. Mol. Biol.* **131:** 435–473.
38. Laggner, P., G. M. Kostner, G. Degovics, and D. L. Worcester. 1984. Structure of the cholesterol ester core of human plasma low density lipoproteins: selective deuteration and neutron small-angle scattering. *Proc. Natl. Acad. Sci. USA.* **81:** 4389–4393.
39. Mayer, E. 1985. Vitrification of pure water. *J. Microsc.* **140:** 3–15.
40. Siegel, D. P., L. Burns, H. Chestnut, and Y. Talmon. 1989. Intermediates in membrane fusion and bilayer/nonbilayer phase transitions imaged by time-resolved cryo-transmission electron microscopy. *Biophys. J.* **56:** 161–169.
41. Frederik, P. M., M. C. A. Stuart, P. H. H. Bomans, W. M. Busing, K. N. J. Burger, and A. J. Verkleij. 1991. Perspective and limitations of cryo-electron microscopy. From model systems to biological specimens. *J. Microsc.* **161:** 253–262.
42. Kahlon, T. S., G. L. Adamson, M. M. S. Shen, and F. T. Lindgren. 1982. Sedimentation equilibrium of human low density lipoprotein subfractions. *Lipids.* **17:** 323–330.
43. Knott, T. J., R. J. Pease, L. M. Powell, S. C. Wallis, S. C. Rall, T. L. Innerarity, B. Blackhart, W. H. Taylor, Y. Marcel, R. Milne, D. Johnson, M. Fuller, A. J. Lusis, B. J. McCarthy, R. W. Mahley, B. Levy-Wilson, and J. Scott. 1986. Complete protein sequence and identification of structural domains of human apolipoprotein B. *Nature.* **323:** 734–738.
44. Yang, C-Y., S-H. Chen, S. H. Gianturco, W. A. Bradley, J. T. Sparrow, M. Tanimura, W.-H. Li, D. A. Sparrow, H. DeLoof, M. Rosseneu, F-S. Lee, Z-W. Gu, A. M. Gotto, Jr., and L. Chan. 1986. Sequence, structure, receptor-binding domains and internal repeats of human apolipoprotein B-100. *Nature.* **323:** 738–742.
45. Yao, Z., B. D. Blackhart, M. F. Linton, S. M. Taylor, S. G.

Young, and B. J. McCarthy. 1991. Expression of carboxyl-terminally truncated forms of human apolipoprotein B in rat hepatoma cells. Evidence that the length of apolipoprotein B has a major effect on the buoyant density of the secreted lipoproteins. *J. Biol. Chem.* **266:** 3300–3308.

46. Phillips, M. L., and V. N. Schumaker. 1989. Conformation of apolipoprotein B after lipid extraction of low density lipoproteins attached to an electron microscope grid. *J. Lipid Res.* **30:** 415–422.

47. Galeano, N. F., R. Milne, Y. L. Marcel, M. T. Walsh, E. Levy, T-D. Ngu'yen, A. Gleeson, Y. Arad, L. Witte, M. Al-Haideri, S. C. Rumsey, and R. J. Deckelbaum. 1994. Apoprotein B structure and receptor recognition of triglyceride-rich low density lipoprotein (LDL) is modified in small LDL but not in triglyceride-rich LDL of normal size. *J. Biol. Chem.* **269:** 511–519.